

ACCESS Pointing Control System

Paul Brugarolas ^{*a}, James Alexander ^a, John Trauger ^a, and Dwight Moody ^a, Robert Egerman ^b, Phillip Vallone ^b, Jason Elias ^b, Reem Hejal ^c, Vanessa Camelo ^c, Allen Bronowicki ^c, David O'Connor ^c, Richard Patrick ^c, Pawel Orzechowski ^c, Connie Spitter ^c, and Chuck Lillie ^c

^a Jet Propulsion Laboratory, 4800 Oak Grove Dr, Pasadena, CA, 91109 (USA)

^b ITT - Geospatial Systems, 800 Lee Rd, Rochester, NY 14606 (USA)

^c Northrop Grumman Aerospace Systems, 1 Space Park Blvd, Redondo Beach, CA 90278 (USA)

ABSTRACT

ACCESS (Actively-Corrected Coronagraph for Exoplanet System Studies) was one of four medium-class exoplanet concepts selected for the NASA Astrophysics Strategic Mission Concept Study (ASMCS) program in 2008/2009 [14, 15]. The ACCESS study evaluated four major coronagraph concepts under a common space observatory. This paper describes the high precision pointing control system (PCS) baselined for this observatory.

Keywords: Pointing, Space Telescope, Coronagraph, Hexapod, Fine Steering Mirror, Fine Guidance Camera

1. INTRODUCTION

Coronagraphic observatories require a very high precision Pointing Control System (PCS) to achieve high contrast imaging of faint objects at extremely small angles from a star during science observations, which typically require long exposures.

The philosophy behind this PCS design has been to propose the best pointing system for a mid-class space coronagraphic observatory with nearly available technology (TRL 6 or above). This led to a three-stage pointing control system; a fine guidance camera design within the coronagraphic instrument; and an extensive disturbance rejection strategy to minimize the environmental jitter. This work is partly based on the work that the authors performed for the Eclipse proposal [1, 2].

The three-stage pointing system starts with a standard 3-axis stabilized spacecraft bus and it is augmented with a hexapod telescope pointing system and a fine steering mirror. The addition of the hexapod enables pointing the telescope with a pointing stability ten times better than Hubble but with a spacecraft bus that is ten times less capable than Hubble. The addition of the fine steering mirror allows for additional pointing capability within the coronagraphic instrument.

For fine guidance sensing we take advantage that coronagraphic observations have a bright star in the center of field of view. We have studied three different concepts for a fine guidance camera that guides from this bright star.

The strategy towards disturbances is to minimize the jitter at the source. We have selected a quiet orbital environment (L2), designed a thermally controlled telescope and instrument, planned operational constraints during science observations (limitations on reaction wheel speeds, non operation of solar array drives and high gain antenna gimbals), and added reaction wheel isolators, solar array dampers and a vibration suppression capability within the hexapod. We have studied two possible options for the hexapod system.

A detail simulation study was performed that included dynamic models of the structure, optics and models for the spacecraft ACS system, the hexapod pointing systems, the FSM and the fine guidance camera to demonstrate the feasibility of this design.

The Pointing Team brings an extensive experience base from three leaders in the Industry. JPL leverages experience from the Spitzer Space Telescope, Kepler and other missions, and from large investments in technology developments for programs such the Stellar Interferometry Mission and the Terrestrial Planet Finder. ITT is a leader in telescope manufacturing and design, and has two decades of investments on the development on pointing and vibration suppression mechanisms. Northrop Grumman brings as well an extensive experience on space observatories (Chandra, JWST, etc.) and many years in development of vibration isolators systems and pointing struts.

2. POINTING REQUIREMENTS

Pointing errors adversely affect image contrast level in two main ways:

- Telescope pointing errors lead to contrast degradation due to wave-front errors associated with beam-walk over the primary and secondary mirrors; and
- Coronagraph occulting mask centering (on the star) errors produce contrast degradation due to light spillage outside the mask.

A detail modeling of the ACCESS coronagraph instrument and science observations (Section 8.8) has simulated the effect of the pointing errors and allocated the pointing stability requirements for the nominal science exposure duration of 1000 seconds.

These allocations define the fine pointing mode requirements for science observations. In particular, the telescope and coronagraph pointing requirements. The telescope pointing stability requirement of 1 mas for the tip/tilt of the line-of-sight (3σ , over 1000 s) drives the need to augment the spacecraft pointing capability with a hexapod pointing stage. The fine pointing requirements were derived for the most demanding science case, which corresponds to the smallest occulting mask with sharp edges. The use of larger occulting masks with optically smoother edges can relax the pointing requirements offering graceful degradation and de-scope options.

The pointing requirements for nominal spacecraft operations and science acquisition are 3-axis pointing accuracy of 30 arcsec (3σ) and pointing stability over 100 seconds of 1.5 arcsec (3σ).

Table 1 shows the pointing requirements classified per pointing mode and control actuation stage used to achieve it.

Table 1. Pointing requirements (angle in the sky, 3σ)

Pointing Mode	Spacecraft Pointing (ACS)	Telescope Pointing (Hexapod)	Coronagraph Pointing (Fine Steering Mirror)
<i>Normal</i> (for SC ops and pointing acquisition)	Accuracy: 30 as		
	Stability/100 s: 1.5 as		
<i>Fine</i> (for science observations)	Accuracy: 30 as (p, y) 30 as (roll)	Accuracy: 1 mas (tip, tilt)	Accuracy: 0.1 mas (tip, tilt)
	Stability/1000 s: 100 mas (p, y), 5000 mas (roll)	Stability/1000 s: 1 mas (tip, tilt)	Stability/1000 s: 0.45 mas (tip, tilt)
		Jitter: 1 mas (<10 Hz) 0.1 mas (>10 Hz)	Jitter: 0.1 mas

3. POINTING ARCHITECTURE

The architecture of the PCS is shown in Figure 1.

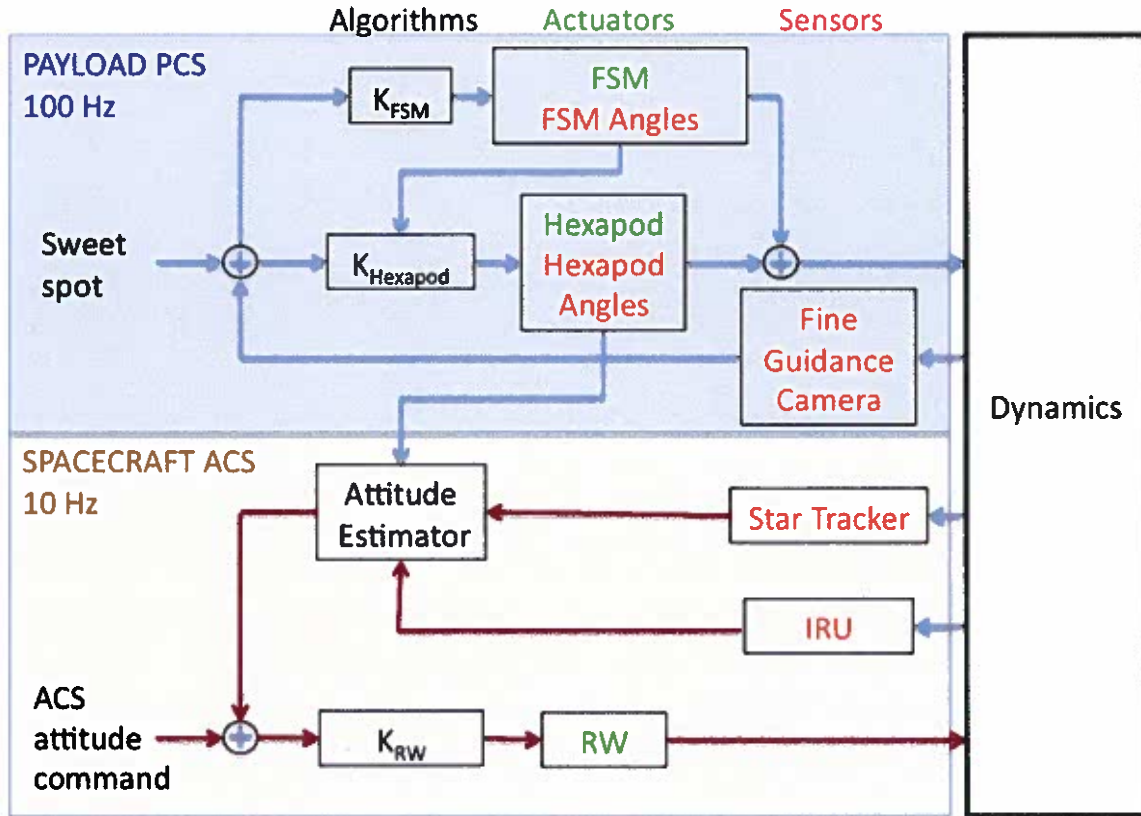


Figure 1. Pointing Control System Architecture

For control we propose a three-stage actuation system. The first stage is the SC ACS - reaction wheel system that stabilizes the SC to 100 mas in pitch and yaw and 5000 mas in roll. This pointing requirement on the spacecraft ACS is within the capabilities of midsize space observatories (Kepler). The second stage is a hexapod telescope pointing system that stabilizes the telescope line-of-sight to 1 mas in tip and tilt (corresponding to pitch and yaw axes of the SC). The hexapod in addition provides a vibration suppression capability. The third stage is the Fine Steering Mirror (FMS) within the coronagraphic instrument that centers the star in the occulting mask to 0.1 mas in tip and tilt.

For knowledge we proposed a fine guidance camera within the coronagraphic instrument that measures the tip and tilt errors. The information from the fine guidance camera is used by an advance control architecture, which commands the FSM and the hexapod. This architecture allows to offload the FSM to the hexapod smoothly and effectively. Basically the FSM loop has a high bandwidth loop that responds quickly to pointing errors, the hexapod has a mid bandwidth, which responds slower and offloads the FSM. In turn, the hexapod is offloaded to the spacecraft ACS by generating a highly accuracy offset angle derived from the hexapod pointing angles. Since the hexapod is tracking the guide star with a precision of 1 mas (1σ) means that a measurement of the hexapod pointing angles is the opposite of the spacecraft pointing error to the same accuracy level 1 mas (1σ). Another way to explain the control architecture is that the hexapod needs to correct for the spacecraft ACS error. Therefore the hexapod has a closed loop bandwidth of about 5 Hz which allows it to reject ACS errors with frequencies bellow 0.5 Hz. In addition the FSM has a closed loop bandwidth of 15 Hz, which allows it to correct for some residual errors at the hexapod stage. The performance has been evaluated in a detailed simulation environment.

The ACS attitude estimator using information from the IRU and the Star Trackers provides the knowledge to control the roll channel. Roll control errors will couple into LOS tip and tilt errors through misalignments and uncertainty on the roll axis. These errors, will manifest as line-of-sight tip and tilt errors with the frequency spectrum of the ACS pointing errors. These errors are within the bandwidths of the hexapod and FSM controllers and will be rejected along with the ACS pitch and yaw errors.

In addition, the selection of high performance optical elements for the optics ahead of the FSM can relax the telescope pointing requirements. If the telescope pointing stability requirement is relaxed to 10 mas, this opens the opportunity to eliminate the hexapod stage by optimizing the spacecraft ACS design to achieve a pointing stability of 10 mas. Other de-scope options are elimination of the fine alignment mechanism to center the PSF at the cross-hairs of four pixels of the fine guidance camera, and elimination of the Fine Steering Mirror.

4. FINE GUIDANCE SENSOR

We have studied three different concepts for coronagraphic fine guidance cameras. The first (Option 1, Spot) was to collect all the light reflected from a coronagraph occulter on to a focal plane, producing a Airy-type point spread function (PSF), allowing almost all of the star light from the central star to be used for centroiding. The second approach, referred to as punctured disk (Option 2, punctured disk) collects the light that bypasses a central obscuration, producing a PSF with a punctured central disk. The final approach (Option 3, Lyot) collects light after passing through the occulter at the Lyot stop.

The “centroiding” performance for each concept is evaluated, making use of both the shape of the star image on the tracking focal plane, and the amount of light that is available as a function of star magnitude for that concept. The term centroiding should not be taken to imply a center of brightness algorithm, but an estimation of image position. The amount of light available to the FGS from a star plays an important role in the overall pointing accuracy. It depends on the particular concept; the Option 2 FGS receives half the light of Option 1, and the Option 3 (Lyot option) FGS only about 1% to 2% of the light of Option 1.

The study included generation of representative images for each option by the science team, followed by an engineering evaluation of a centroiding or a photometric algorithm for each option. The options are described in more detail:

Option 1: Light reflected from the occulting mask is picked off and sent to the tracking focal plane. An advanced centroiding algorithm that incorporates a model of the Point Spread Function (PSF) is used for the position estimation process. This option requires making use of the fine alignment stage of the fine guidance selection mirror to center the PSF within 15% of the crosshairs of four adjacent pixels to make the position estimate more sensitive to small changes of the image location. An additional key requirement is that a reference centroid x-y point on the tracking detector needs to be determined that represents the optimal pointing for the coronagraph. Since this is not a direct measurement, simultaneous measurements of the coronagraph and FGS are needed as part of an alignment procedure. A representative image of the raw PSF is shown in Figure 2 (left).

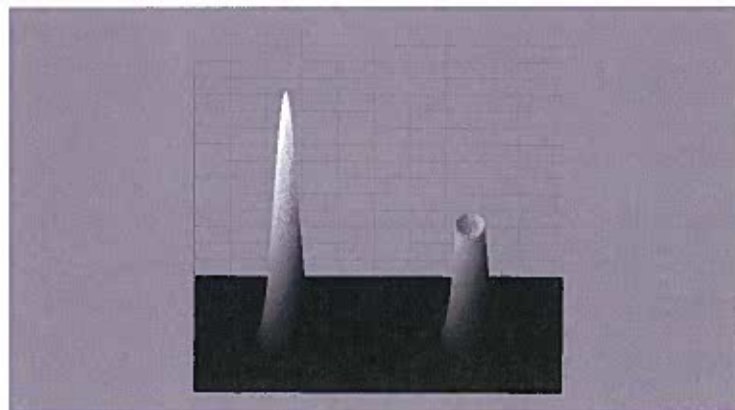


Figure 2. Option 1 and 2 3-D PSF

Option 2: Light reflected from the circular occulting mask is picked off and sent to tracking focal plane. The central occulting mask makes the resulting PSF look like a punctured version of the Option 1 PSF. A representative image is shown in Figure 3. The image used for tracking has roughly 50% of the light acquired in Option 1. Additionally, as in Option 1, a separate alignment procedure is required. A photometric centroiding algorithm that evaluated the variation of intensity with pointing error was used for the analysis. While losing half of the light, this approach has the benefit of removing the high central region, reducing the dynamic range needed on the detector, and additionally providing a sharp transition area, (the dark central disk), which can be used to make more sensitive measurements. This case is analogous to the proposed PIAA coronagraph low-order-wavefront-sensing concept [3]. The overall performance of this approach appears (to be shown later, see Figure 8.5.4-6) slightly worse than in Option 1. However, this approach reduces the risk of the detector becoming saturated by images created by bright stars using the Option 1 approach, and should be considered in new trades. Figure 2 showed a direct comparison (linear scale) between images from Option 1 (left) and Option 2 (right). Note the central cylindrical volume of right PSF (Option 2) has been eliminated with respect to the left PSF (Option 1).

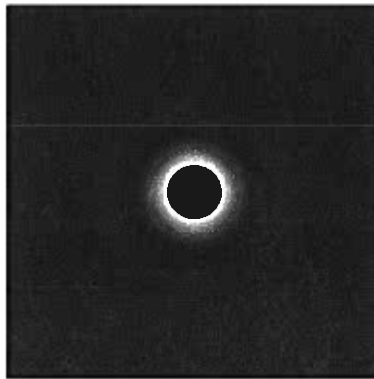


Figure 3. Option 2 2-D PSF for the punctured disk

Option 3: Light reflected from the Lyot stop is picked off after the light has passed through a linear occulting mask. A representative image is shown in Figure 4. A photometric technique was used in this case to evaluate the pointing performance. Here the image used for tracking directly represents the light used by the coronagraph (both images discard the central portion of the star image), and the alignment becomes significantly easier. A downside is that some of light used by the coronagraph is required for the tracking measurement. Currently 10% of the coronagraph light, plus the longer wavelengths (to about 950 nm) is sent to the tracking focal plane. The total light provided for tracking purposes is only about 1% to 1.5% of the light obtained by Option 1.

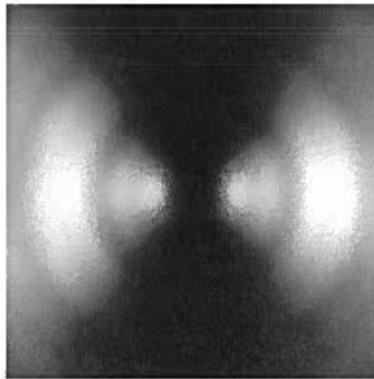


Figure 4. Option 3 2-D PSF

Figure 5 shows a set of images obtained by moving the PSF in 0.1 mas increments across the occulting mask. The images displayed are computed to be the difference between an offset pointing image and a zero offset pointing image (which was shown in Figure 4). Visual inspection of these images shows the sensitivity of this technique to measure pointing errors.

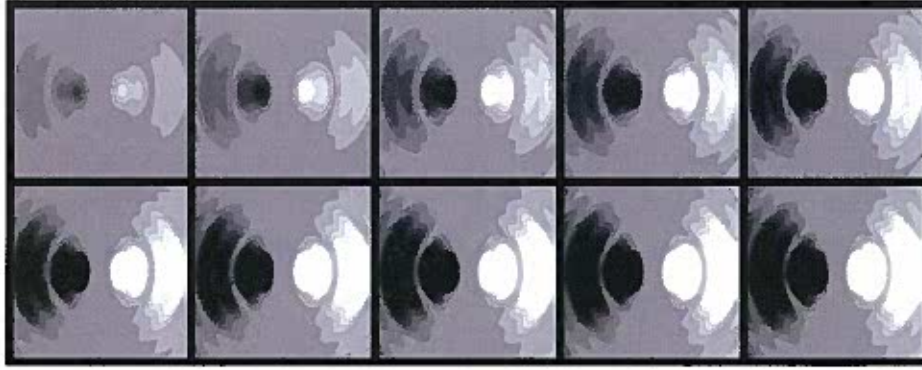


Figure 5. Option 3 Photometric incremental sensitivity to pointing errors; the image is simulated moving from left to right in 0.1 mas steps. The rapid change of relative signal intensity highlights the “shape” sensitivity of this approach to motion.

The results of this trade study are shown in Figure 6 and summarized in Table 2 for star magnitudes 3 and 7. The performance of course depends largely on the photons available for guiding, which is limited by the FGS design. All options were evaluated assuming a 0.01 second integration window to support a 100 Hz fine guidance camera measurement update. Option 1 has a very large number of photons available to it because of the large aperture of the telescope and the brightness of the star. Option 2 has about half the photons of Option 1. And because Option 3 has only about 1% of the photons of Option 1, Option 3 did not address the magnitude 7 star case because the photons available could not support a 100 Hz measurement rate.

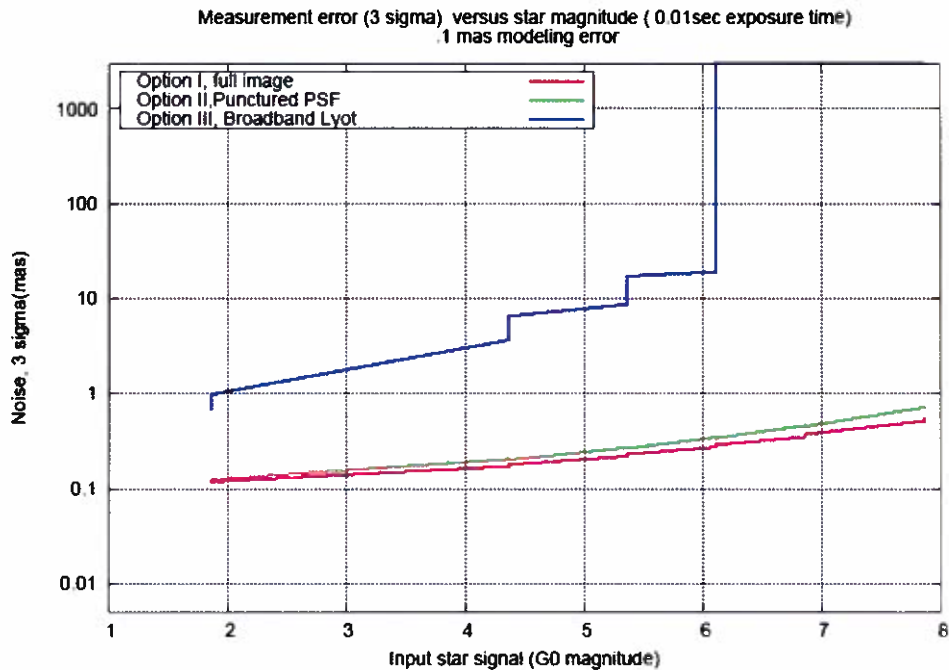


Figure 6. Centroiding performance for Options 1 to 3 for Fine Guidance Camera concepts versus star magnitude (G type stars).

Table 2. Pointing performance of Fine Guidance concepts (angle in the sky, mas, 3σ)

	Star Magnitude 7	Star Magnitude 3
Option 1: Centroiding on reflected image	0.3	0.18
Option 2: Photometric Technique punctured-PSD	0.3	0.18
Option 3: Photometric Technique at Lyot after occulting mask		2.1

The assumed signal (measured in electrons/per second from the detector) as a function of star magnitude (option 1, magnitude 7 used as a reference) is presented in Table 3. The amount of signal available for a magnitude 7 star for Option 1 is roughly 100,000e. The signal available for Options 2 and 3 uses the same optical and detector efficiency and the additional effect of the masking.

Table 3. Signal levels for Fine Guidance concepts

Signal/ electrons per 10ms			
Magnitude (G0 star)	Option 1 PSF	Option 2 Punctured PSF	Option 3 Lyot
10 ms exposure			
0	63,348,416	31,674,208	633,484
3	3,997,015	1,998,507	39,970
5	633,484	316,742	6,335
7	100,400	50,200	1,004
9	15,912	7,956	159
11	2,522	1,261	25

Option 1 has been selected as the baseline because it is independent of the type of occulting mask used and provides the best overall performance. Option 2 and 3 will require specialized photometric algorithms for each type of mask.

Overall noise is illustrated in Figure 8.5.4-6. Modeling error accounts for roughly 0.1 mas error; it is possible that this could be improved by more detailed modeling. The bulk of the remaining error is noise and image jitter over the exposure period.

Spot Centering, Centroiding Approach

After the alignment of the coronagraph to the fine guidance system, a “nulling” point on the FGS focal point is determined by calibration, such as shown in Figure 8.5.4-7.

This alignment is implemented by a fine alignment mechanism that is part of the Fine Guidance Camera selection mirror (see Section 8.6 for additional information).

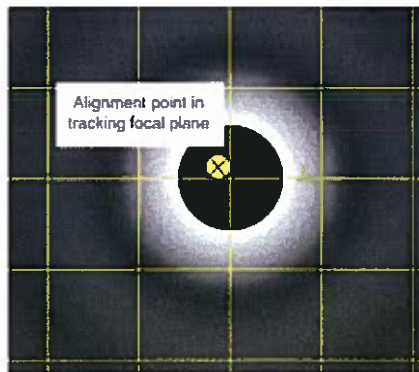


Figure 7. PSF is shown aligned to the cross-hairs of 4 FGS pixels. The “X” represents the point to which the center of the dark disk needs to be placed to optimize coronagraph performance. The thin yellow grid lines are the pixel boundary. As shown, the offset of the optimal pointing location from the cross-hairs of 4 FGS pixels is roughly 15% of a pixel, which is the desired alignment requirement.

If the star image meets our modeling assumptions, and the star “centroid” can be driven to that nulling point shown in Figure 8.5.4-6, the contrast for the coronagraph will be maximized. For Options 1 and 2, the nulling point is determined by making coronagraph measurements on a bright star (to shorten the integration time), and determining physical point in the tracking focal plane, such as shown that maximizes the contrast. For the Lyot Option 3 case the alignment is

significantly easier. For each case, image models are built, to describe the change of star signal (the photometric sensitivity) as the star moves from the nulling point.

In all the cases, our model evaluates the change in the star signal in the pixels, and uses the change to determine a correction factor. Because the alignment point is fixed, and the control system maintains tight pointing control, (better than a few milliarcseconds), the change in star signal as a function of displacement from the alignment reference point can be linearized, resulting in less than 5% error in the resulting correction term (displacement errors of 1 mas would result in less than 0.05 mas error). Most of the important signal for centroiding is in the 2×2 to 4×4 region around the alignment point with a pixel size of 70 mas. Figure 8.5.4-5 illustrates the change of image signal with displacement for the case of Option 3.

A variation of options 1 and 2, which could be used if only bright stars—those brighter than magnitude 9—were observed as science targets, would be to spread the image over a full 10×10 or larger pixel area, creating a smaller angular pixel size, and digitally rebinning the data to maintain a simple nulling algorithm. The alignment requirements relative to the pixel boundary could then be relaxed, since the pixel size could be <25 mas. This has the downside that the pixel read noise plays a much larger role ... the number of pixel measurements would grow by factors of 25 to 100. A more complicated algorithm, which uses optimized weights for each of the pixels has been previously looked at, but requires significantly more calibration effort, and has more color dependence as the pixels get further from the center.

5. STRUCTURAL DESIGN

The spacecraft (SC) structure provides mounting interfaces which meet field of view (FOV) requirements, and maintenance of critical alignments for the telescope and SC bus components of the ACCESS space segment with a configuration that fits within the launch vehicle static envelope.

The SC bus consists of a primary structure supporting the propulsion module, spacecraft equipment panels, payload panels, and solar array assemblies. The easy-to-build, test-proven, modular design maximizes equipment accessibility and integrates passive thermal control. The all Aluminum SC structure is efficient, lightweight, and has high-stiffness.

The structural dynamic characteristics of the SC are designed to meet the minimum frequency requirement specified by the launch vehicle supplier, to support the vibroacoustic responses of the mounted payload and SC bus equipment, and to minimize jitter response at the payload interface (I/F) during operation within acceptable limits.

The SC structure is designed to have sufficient strength to react loads derived by a Launch Vehicle-observatory coupled loads analyses and additional vibroacoustic loads with the applicable factors of safety.

Deployables solar array (SA) panels and associated tie-down and release devices provide the required SA stiffness for launch. The SC bus structure includes the Propulsion Module, the equipment panels, a two-wing solar array with tie-downs and release devices, and miscellaneous loose brackets.

The propulsion module encloses the propellant tank and uses a central cylinder to carry the primary structural loads. The central cylinder offers an efficient structural load path from the payload to the LV. The central cylinder and cone are based on the heritage EOS design, with a transition cone to the launch vehicle interface. Panels and fittings support the propellant tank inside the central cylinder/cone.

Similar to the GeoLITE heritage design, vertical and horizontal shear panels provide the interface between the equipment panels and the central cylinder.

The equipment panels are dedicated to providing support and thermal protection of the SC electronics equipment and spacecraft batteries. The equipment panels are aluminum honeycomb and contain embedded heatpipes, similar to GeoLITE, and are attached to the spacecraft structure by titanium flexures. This allows the use of lower-cost aluminum panels in place of composites without impacting spacecraft dimensional stability.

The mounting interface with the Payload Support Bi-pod Struts is at the intersection of the three vertical shear panels with the +Z platform. The interface fittings transfer load from the payload to the vertical shear panels, which provide a direct load path to the central cylinder.

The SA Mechanical Assembly is based on the GeoLITE design and consists of two wings with three panels each, which fold in a flat-pack configuration, with cable-activated latch/release locations per wing.

Structural Model

Analytical Finite Element Models (FEM) of the SC bus have been generated for the stowed and deployed configurations to verify design feasibility for launch and on-orbit performance (Figure X). The stowed model was used to verify minimum frequency stiffness requirements and to provide initial sizing for structural mass estimates. The deployed model is derived from the stowed model and was integrated to the telescope model provided by ITT to perform on-orbit jitter and controls trades to verify design feasibility to satisfy on-orbit performance requirements.

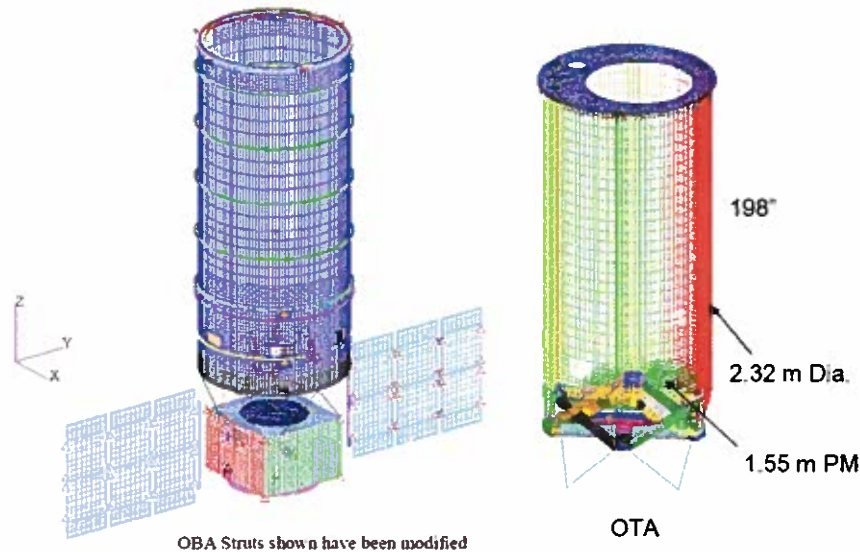


Figure 8. Finite Element Model.

The analytical model generated represents the current design consisting of the central cylinder spanning the SC height from the LV interface adapter to the PL platform. Shear panels radiating from the central cylinder to the equipment panels are included. Equipment panels are attached to shear panels and the upper and lower platforms. Equipment mass has been included based on current mass properties defined by various subsystems.

Two versions of the SC design have been modeled, a rectangular and a hexagonal bus. In both cases launch feasibility has been verified by initial sizing that satisfies the minimum lateral frequency requirement of the LV with the payload supported by the SC. The hexagonal bus offers a more efficient structure for the PL and has been adopted in the baseline design. The two bus models have been integrated to the telescope model provided by ITT.

A detailed model of the SC bus is included. The central cylinder is of composite construction, while the equipment panels are of Al Honeycomb construction. The telescope is supported by the SC via six (6) struts in a kinematic arrangement, an hexapod. The struts have been angled and sized to obtain a fundamental lateral frequency of about 15 Hz when fixed at the strut end to SC. The struts are intended to be supported directly by the primary structure for an efficient load path. This enables the observatory launch frequency to be above the minimum lateral frequency requirement of the LV. Two versions of the struts have been considered. The NG active/passive struts and the ITT AIM struts.

Each SA wing was modeled per current design to include three (3) panels that are stowed and locked via launch locks to the equipment panels. In its deployed configuration, each SA panel is attached to the adjacent panel via tape hinges with significant flight heritage. The three-panel solar array design has flight heritage in the GeoLite program. The solar arrays models are from the GeoLITE program and are at 0.3 Hz.

The integrated deployed FEM includes the SC, the telescope, and the deployed SAs. SC Mass properties were based on current mass properties estimates with 43% contingency. The telescope model was supplied by ITT and contains representations of Beam Walk (BW) LOS X and Y. The TS Mass properties are from ITT supplied FEM. The integrated model contains simplified models of the reaction wheels and their isolators as described below. The SC hexapod APSI isolator offers 6 degree of freedom isolation between 0.5 and 2 Hz. The current model is based on Control/Structure

Interaction (CSI) testbed design of the long stroke isolators. The integrated model has been checked for grounding, particularly a LOS rigid body check has been performed and found acceptable.

A summary of the integrated deployed model development is shown in Figure 8.5.5-3. The integrated FEM is also shown. The integrated model was used to determine modes up to 300 Hz to account for high frequency wheel harmonics. The model is in English Units (mass is in lbf-sec²/in), but metric versions have also been generated of the SC side. The integrated FEM as well as open and closed loop state space matrices have been provided to JPL for use in dynamics and controls trades.

In summary, the integrated ACCESS model was used to determine jitter performance due to wheel disturbances. Beam Walk (BW) LOS equations were represented in the TS model via MPC equations supplied by ITT based on their current optical design. A detailed RW disturbance model representing fundamental and higher wheel disturbance harmonics for all RW disturbances was used in the analysis. The RW disturbance model, which is based on Teldix RDR 68 measurements from the Chandra program, was used in the detailed jitter analysis. The disturbance model was provided to JPL and ITT as well. Refer to the enclosed package for RW disturbance model details.

6. VIBRATION ISOLATION

ACCESS has very stringent jitter and pointing requirements. Jitter above 10 Hz must be below 0.1 mas, while the pointing stability requirement is 1 mas.

Our approach to meeting the stringent on-orbit jitter budget is to utilize a dual stage isolation scheme between the main sources of jitter disturbances from the reaction wheels (RW) to the PL. Mounting the RWs on specially built passive isolators designed to attenuate wheel imbalances and disturbances in lateral, axial and bending degrees of freedom (DOF) provides the first stage of isolation. An hexapod assembly supporting the TS to the SC structure with vibration isolation capability serves as the second stage of isolation. Two options for the hexapod design have studied (vid. Section X)

Jitter response was evaluated using a dynamic model of the on-orbit configuration with a TS model. Analyses showed that employing the dual stage isolation provides the attenuation necessary in a wide frequency range above 1 Hz. The dual stage isolation scheme also provides reduced risk of not meeting error and jitter budgets as it minimizes the sensitivity to modeling errors and modal interactions between the SC and the TS.

NGAS has been successful in building passive isolators that are simple, compact and light and meet stringent on-orbit performance requirements. Flight-proven design heritage from previous NGAS programs will be applied in the design. The Chandra wheel isolator and EOS SADA joint damper described herein are examples of successful passive isolators designed and flown by NGAS.

Reaction Wheel (RW) Isolator

The only significant source of jitter from the SC to the TS is due to the RW disturbances. These are due to RW static and dynamic imbalances and bearing noise disturbances which occur along five (5) degrees of freedom (DOF). Each RWA is mounted on an isolator of Chandra heritage (Figure 9). The RW Isolator Assembly (RWIA) provides the 1st stage of isolation of the wheels in all 5 degrees of freedom of wheel disturbances. Each RWIA consists of six machined Titanium springs fitted with Visco-Elastic material (VEM) to provide damping close to 5%. The RWIA springs have a load alleviation passive mechanism that provides damping and graceful load isolation for launch. This furnishes a soft ride for the RWs during launch which has proven to minimize vibrations into the RWs that tend to worsen RW disturbances.

The RWIA is designed to include two rocking modes around 6.7 Hz, followed by an axial mode around 9 Hz and the 2nd lateral/rocking modes around 11 Hz. The RWIA torsional mode is around 21 Hz. The RWIA has no modes of significance above 11 Hz and offers excellent isolation of wheel disturbances as demonstrated by transmissibility testing on the Chandra program. A simplified, test validated RWIA model has been included in the Access integrated model. The RWIA isolator model has been validated by comparing its predicted axial, lateral moment transmissibility to those measured on the Chandra program. Refer to the enclosed package for additional details on the RWIA.

Four wheels are included and have been oriented in the model per ACS requirements. The RW/RWIA assemblies are mounted via stiff RWA brackets to the central cylinder close to the shear panels interface.

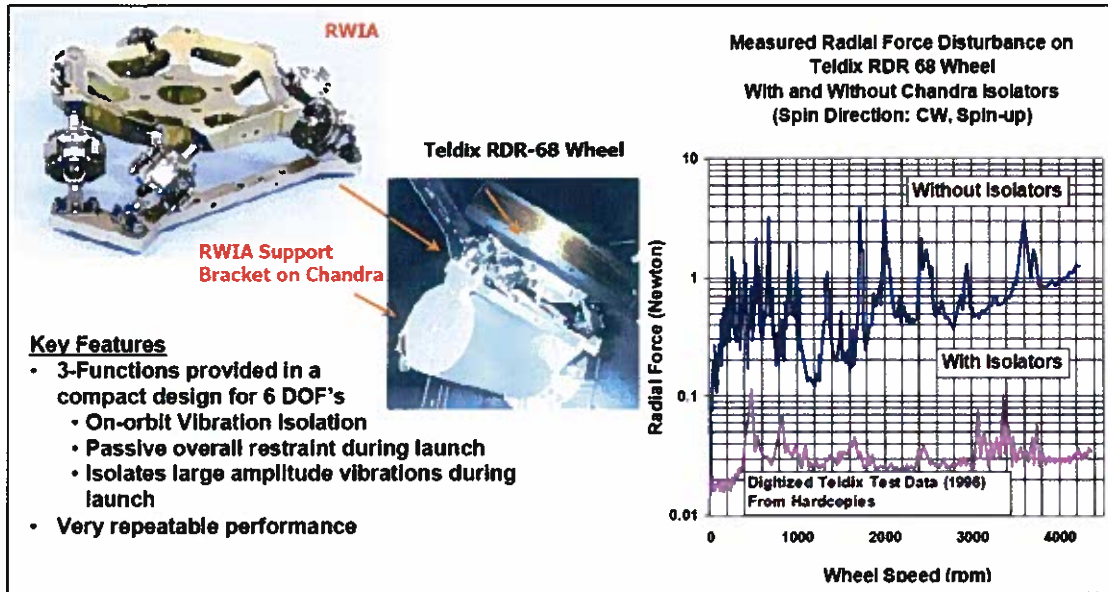


Figure 9. Reaction Wheel Isolator Heritage Chart

Solar Array Joint Damper

An optional joint damper may be utilized to provide damping of low frequency Solar Array (SA) modes that may potentially couple with the controls bandwidth. The joint damper is of flight heritage in both EOS AQUA and AURA (Figure 10). It consists of a series of flexures and fitted with VEM for damping. The joint damper is attached to the SADA on one end and the SA yoke on the other end. Damping characteristics have been measured on for a wide range of temperatures and the choice of VEM will be selected based on ACCESS thermal environment.

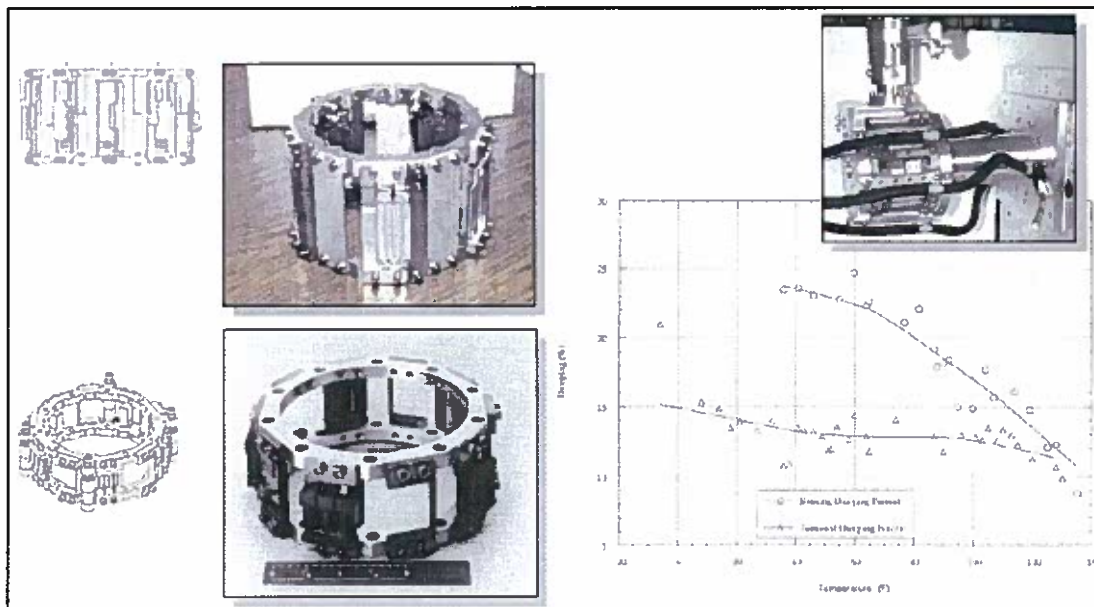


Figure 10. Solar Array Joint Dampers

7. SPACECRAFT ATTITUDE CONTROL SYSTEM (ACS)

The ACCESS inertial referenced attitude control system (ACS) is shown in Figure 11.

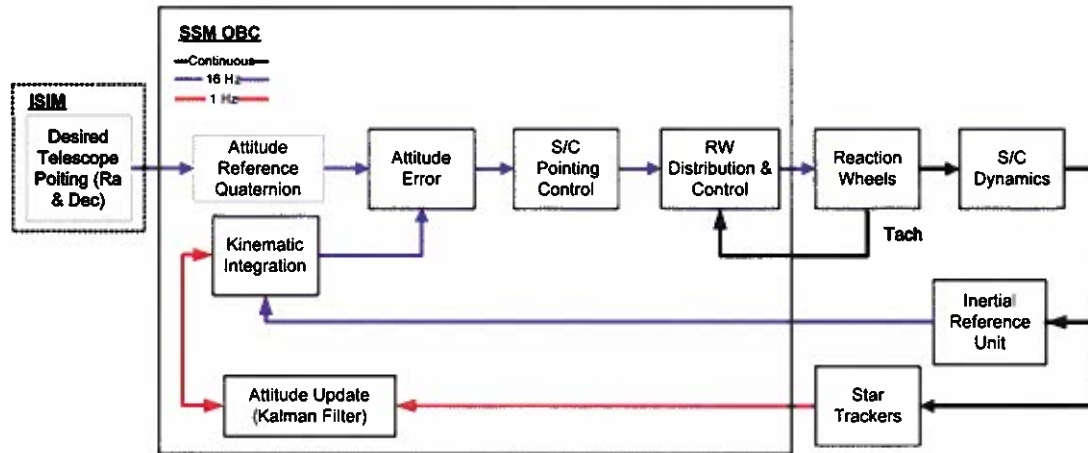


Figure 11. Integrated Pointing Control Architecture showing the ACCESS Observatory ACS

The ACCESS ACS utilizes star trackers and IRUs for attitude determination, and reaction wheels for control. The ACS loop topology per axis consists of a Proportional + Integral + Derivate (PID) compensator, a second order bending filter to attenuate flexible modes, a momentum control loop for reaction wheel control, and an IRU (4 Hz bandwidth) for body rate information. The on-board attitude information is maintained and propagated as quaternions, by performing the kinematic integration using IRU data. In addition, a Kalman filter is used at a slower rate to correct the IRU drift and the estimated attitude quaternion by using star tracker measurements referenced to a star catalog.

The ACCESS ACS uses a momentum exchange system which consists of a 4 reaction wheel cluster configured in a pyramid configuration to provide balanced momentum storage capability in each of the three spacecraft axes. The momentum control loop consists of a Proportional+Integral (PI) compensator, a first-order low-pass filter, a tachometer, and a tachometer-averaging filter for each wheel. The reaction wheels can be set to a bias by using an additional bias control loop that regulates reaction wheel speed operation near a fixed speed in the null-space of the RWA cluster. This RW bias speed is chosen to minimize structural vibration excitation.

The ACS hardware models such as the reaction wheels, reaction wheel speed tachometer, reaction wheel disturbance models, and inertial reference units (IRUs) are all taken from JWST. The ACCESS spacecraft dynamics are modeled as a rigid body with flexible body modes superimposed.

8. TELESCOPE POINTING SYSTEM

Two telescope pointing systems have been studied: ITT Active Isolation Mount System and NGAS Active/Passive Spacecraft Isolator.

ITT Active Isolation Mount System (AIMS)

The Active Isolation Mount System (AIMS) was designed in the late 90s to serve two purposes: 1) to reduce transmission of bus-borne vibrations into the payload and provide damping to the payload modes, and 2) to enable fine 6-DOF (Degree Of Freedom) pointing control. The AIM system traditionally replaces the kinematic mount between the bus and payload. This implementation was used for the ACCESS study. AIMS hardware technology, including the associated AIMS Control Electronics has been flight qualified and has a NASA Technology Readiness Level (TRL) 6.

The dynamics lab located in Rochester NY, houses a fully functional 2.5meter-class dynamic testbed. This testbed is comprised of a flight-like telescope built with flight-traceable graphite-composites and it includes an aluminum bus simulator with in-class dynamics. The telescope mass is ~570 kg (1250 lbf) and the bus mass is ~1135 kg (2500 lbs).

AIMS sits in between these two major subsystems and serves as the primary vibration attenuation stage between the bus and payload. A photo of the setup is shown in Figure 12.

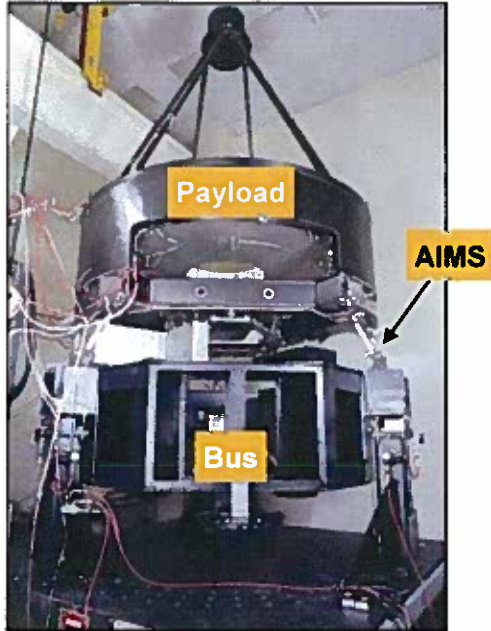


Figure 12. Dynamics Testbed and AIMS Photos

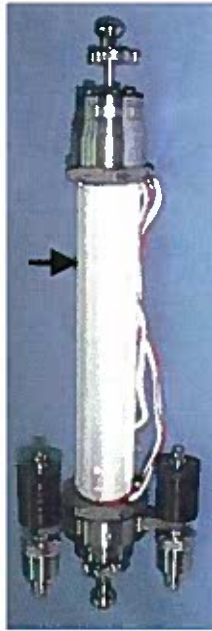


Figure 13. Gen-2 Active Isolation System



This bus-payload testbed has been highly characterized via detailed modal surveys of both the bus simulator and payload. There are 65 seismic accelerometers on the payload to measure the key performance parameters of LOS jitter and the primary mirror's wave-front error (WFE). The photo of the AIMS strut shown above is the *third generation* of active isolation struts. The first generation was built in the early 1990s. It was built very quickly in 10 months as a proof-of-concept for active vibration isolation. The performance was sufficient to show merit and the idea received further funding. A year later, the build of gen-2 active isolation began in collaboration with JPL and Draper Labs. This strut was significantly more refined and performed significantly better than the 1st generation. The JPL work was done under the direction of Dr. Robert Laskin. The testbed system that gen-2 was installed in is shown in Figure 13. (Note: this testbed has been reconfigured for other purposes)

The gen-2 strut had two significant issues:

1. Its ability to survive a launch was risky due to the use of a PZT stack. A stack has excellent load capabilities in compression, but very poor load carrying ability in tension. Displacement stops could have been implemented to reduce the risk, but they'd potentially introduce additional shock loads right when other dynamic loads are at their highest, keeping the solution at a high risk level. Preloading was considered, but this essentially doubles the compression load, reducing the robustness of the system. Launch locks could have been implemented as well, but they'd introduce another failure mode.
2. A PZT stack has significant hysteresis. This non-linearity can cause a transfer-function measurement of stability to appear acceptable at one input level, but change at another input level such that it was very difficult to accurately determine stability margins. A 6dB margin at one level can become only 3 dB at another input level.

However, even with these design shortcomings, the performance of this strut showed the merits of active vibration control. The AIMS was designed to address the gen-2 shortcomings (design is shown in Figure 12). The AIMS system has been developed and verified to a Technology Readiness Level of 6, including the hardware, control electronics, and software. Determination of pointing accuracy will have to be done in a vacuum chamber to eliminate air turbulence and reduce thermal disturbances from corrupting the data. ACCESS's 5 nrad 3 σ pointing requirement will require such a test environment, and additionally this environment must be dynamically quiet. ITT has such a facility [[ACCESS Rep. Ref](#)]

AIMS performance on the ACCESS Observatory. A controller was designed for the vibration control (VC) based around the 1st generation of ACCESS spacecraft (bus + payload) model. This model was not optimized and therefore the VC was not overly refined. Performance of the VC was verified and showed that the 0.5 nrad/s of jitter, defined as LOS motion greater than 10 Hz, could be met but only for a very small range of wheels speeds (RPMs) for the preliminary design. The degree of wheel speed restriction is not likely to be acceptable. Fortunately, just as this report was being written a new NASTRAN model of the telescope with updated representations and Outer Barrel Assembly (OBA) struts of the OTA Aft Metering structure, was integrated with a new NASTRAN model of the current baseline ACCESS bus design (which is hexagonal and considerably larger than the 1st bus design analyzed) and used to generate some additional results. It shows better open loop jitter performance than the previous system model. Part of this improved performance can be credited to the larger bus design enabling a more efficient interface between the OBA and the spacecraft in terms of strut mass and load path. Unfortunately, this favorable pairing of bus + payload was not available for the subsequent analysis, but it is *important to keep in mind when reviewing the results that follow.*

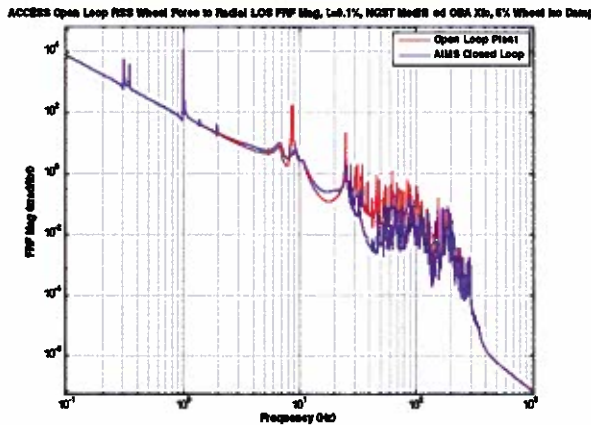


Figure 14. Frequency Response from Wheels to LOS, Open (red) vs. Closed Loop

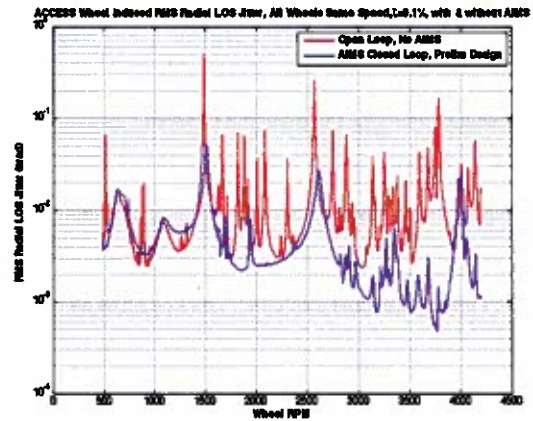


Figure 15. LOS vs. Wheel RPM, Open vs. Closed Loop

The payload's response to wheel disturbances was modeled by bringing the NASTRAN model into Matlab in state-space form. Modal damping of 0.1% was assumed on all modes except the reaction wheels. This is the model that was used to analyze jitter from the wheels. Later, 5% modal damping was applied to all solar array modes below 2Hz; this model was used for the pointing control analysis (Note: results shown above are with lightly damped solar array modes). The AIMS vibration controller was then closed around the appropriate I/O of the plant state-space model. Open loop vs. Closed loop performance (wheel to LOS) is shown in Figure 14. From the closed loop transfer function, it is clear that the 25Hz mode will be dominant in the jitter response. This frequency corresponds to a wheel speed of 1500 RPM. Subsequent efforts could optimize this mode for better controllability and/or localized control. Wheel disturbances were then analyzed over all wheels speeds and LOS results are shown in Figure 15.

As seen in Figure 14, significant isolation doesn't start until approximately 30 Hz. A higher gain controller can be designed that will give better isolation, but for conservatism this lower gain controller was kept. That is, the peak loop gain of this controller is ~31 dB; for reference the loop gain used on the demo payload/bus system in the dynamics lab in Rochester NY is ~55dB. A 4X performance increase over this baseline 31 dB spacecraft/controller design is achievable, and a 5X performance increase is not out of the question. The key will be to do the design as an integrated effort, with all components optimized to reduce jitter. It is likely that jitter will be one of the most difficult program-level specs to achieve.

An *estimated* jitter performance is depicted in Figure 16 into account 3 system design improvements:

1. Reduction of the wheel isolation frequency from 6 Hz to 3 Hz to yield approximately a 4x overall jitter reduction
2. Use of Proof-Mass Actuators (PMAs) to reduce key jitter producing components, like the SMA
3. Refinement of the AIMS controller in light of changes 1 and 2.

The green shaded box at the bottom of the graph in Figure 16 indicates at what reaction wheel frequencies the system meets the specification given the above assumptions. One can see that the allowable wheel speeds have increased significantly, but large keep out zones still exist. An integrated payload and control system design optimization performed at a future date should increase the allowable wheel speeds to greater than 90%.

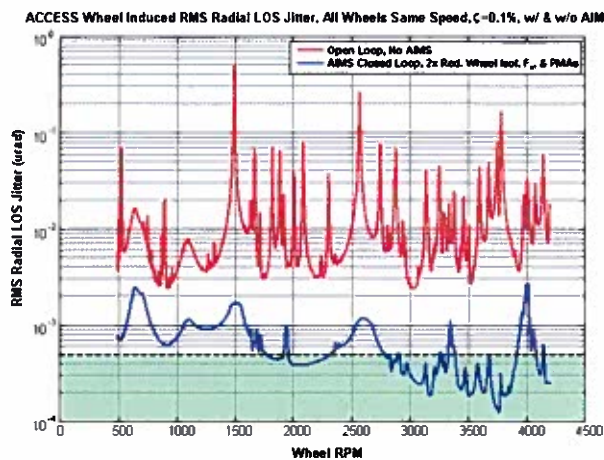


Figure 16. Wheel Jitter with Projected Improvements, *Excluding System Optimization*

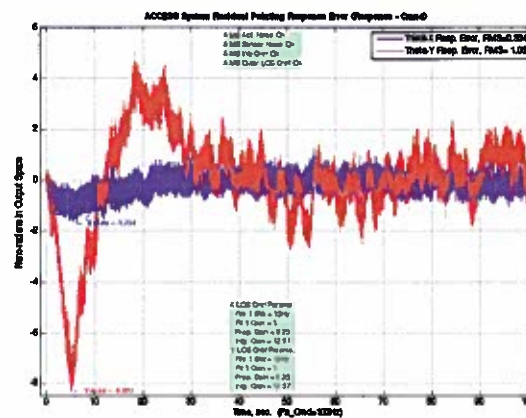


Figure 17. With minor design changes, the residual pointing error will meet the ACCESS 5 nano-rad requirement

In summary, significant work was done on the ACCESS study to integrate the AIMS into the Pointing Control System (PCS) Architecture. The baseline controller with a peak loop gain of ~31dB was deemed usable as is for augmentation with pointing control. The AIMS VC was augmented with the Pointing Command (PC) generation blocks provided by JPL. Numerous analyses were performed to understand the pointing errors, which culminated in the data shown in Figure 17. In conclusion, sufficient ACCESS specific analyses (which leverage techniques that have been correlated to a flight-like dynamics test bed) have been performed to demonstrate that a pointing control system that includes the AIMS and local damping treatments can be optimized to meet the ACCESS line-of-site and jitter requirements.

NG Active/Passive Spacecraft Isolator (APSI)

The 2nd hexapod option is Northrop Grumman's active/passive SC isolator (APSI). The APSI consists of a passive isolator stage consisting of six (6) springs arranged in a hexapod configuration to provide isolation in all 6 degrees of freedom. The 6 springs are attached to the TS struts at one end, and on the other to the SC upper platform/shear panel/central cylinder fittings. The passive isolation is achieved through stiffness of flexure spring and is easily tunable. The APSI struts have been sized in the integrated model to lead to isolation frequencies from 0.5 to 2 Hz. Damping is provided via VEM fitted around the spring. The passive isolator is a scaled version of the heritage Chandra wheel isolator described above. As such, the passive stage of APSI is considered to be of a high TRL maturity.

A long stroke version of the APSI has been demonstrated on the Control/Structure Interaction (CSI) testbed at NGAS (Figure 18). The APSI design is at least of TRL 5 maturity and a preliminary plan to bring its maturity to TRL 6 has been developed. A summary of long stroke isolator and plan to TRL 6 upgrade is shown.

For launch, the struts will be locked to provide stiffness requirement for launch. Low shock, high-strength capability, commercial release devices will be used to provide the restraint needed for launch.

A jitter analysis of the passive isolator capabilities demonstrates that the 0.1 mas maximum jitter requirement is achieved in a wide range of wheel rates below 6000 rpm. Jitter requirements would not be met if the APSI isolator is not included. This is clearly demonstrated in Figures 19.

The passive struts are augmented with an active stage to provide the 50:1 attenuation of SC ACS pointing error required. A voice-coil is housed within each of the spring assemblies and is attached kinematically to the springs via upper and lower specially designed flexures. The voicecoils are commanded to adjust the struts based on FSM angles, providing a stable platform that minimizes FSM center movements to 1 mas.

- **Implemented on IRAD on CSI Test-bed & capability partially demonstrated**
 - PC-based dSpace multi-axis controller
 - No optical Elements
- **Active payload Pointing mount + Passive Isolation in 6 DOFs**
- **28 lb actuators (4 lb/amp) + large gaps in main spring enable 14 mm long stroke**
- **PZT load ring from TRW active auto suspension with special charge amp (μN sensitivity)**
- **Long stroke capacitive sensor for attitude transfer with $\mu\text{-meter}$ sensitivity**
- **VEM damping pads applied to individual spring flexures to dampen local resonances while preserving compound spring-damper performance**
- **Overall Characteristics**
 - Long stroke (± 7 mm at strut level, ± 1 deg at payload level)
 - Sized to provide 1 Hz bounce mode of 900 kg payload
 - Other damping options: back EMF, force feedback
 - Internal volume sized to accept even stronger actuator
- **TRL 6 Readiness requires full demonstration of capability**
 - Flight-like electronics
 - LOS Detection & Performance Demonstration
 - Launch Lock development




Figure 18. Northrop Grumman Active Passive Spacecraft Isolator (APSI)

Strut adjustment command is achieved using Independent Modal Space (IMS) Control to distribute commands to strut actuators using the fundamental isolation mode shapes. Because the fundamental isolator modes are easily measured, this scheme is very easy to implement and provides minimal risk. As such, this design is very advantageous as it is unnecessary to have knowledge of high frequency modes, and is insensitive to plant dynamics since the active part does not interact with higher TS modes. Actuator commands for LOS X and Y are decoupled with four orders of magnitude separation as seen in Figure 20.

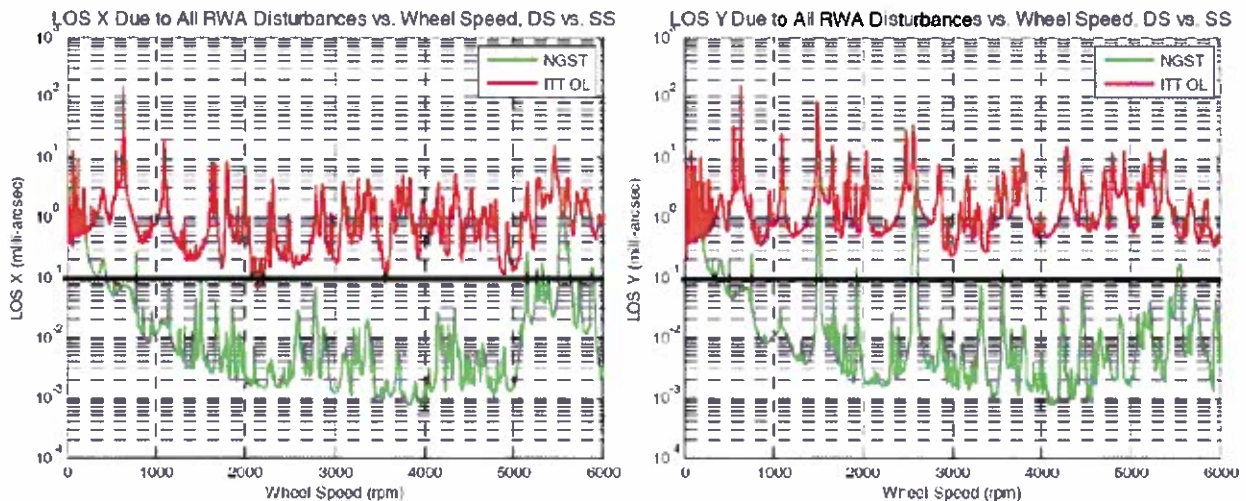
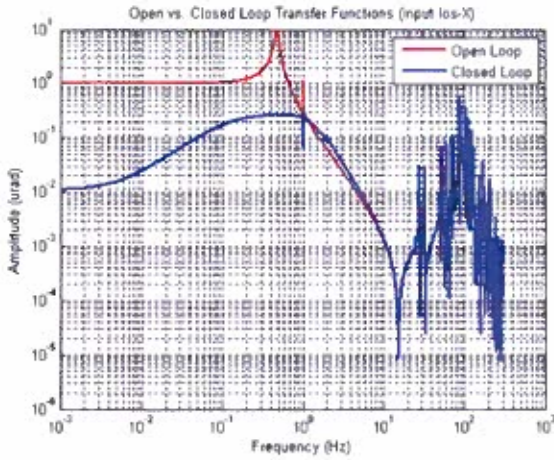


Figure 19. Line-of-Sight jitter versus Reaction Wheel speed plot showing comparison between NG passive isolator capability (*green*) in relation to rigid struts (*red*)

LOS X command input to LOS X measurement



LOS Y command input to LOS Y measurement

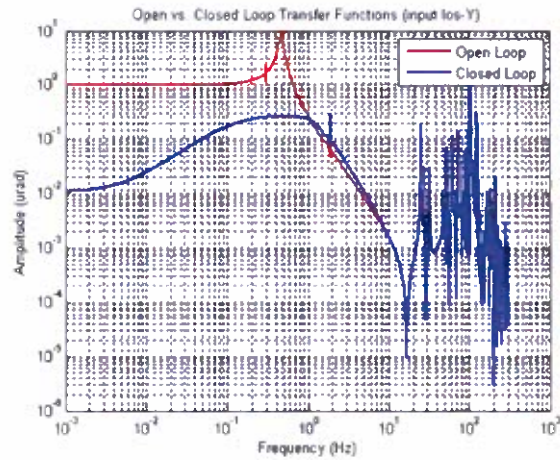
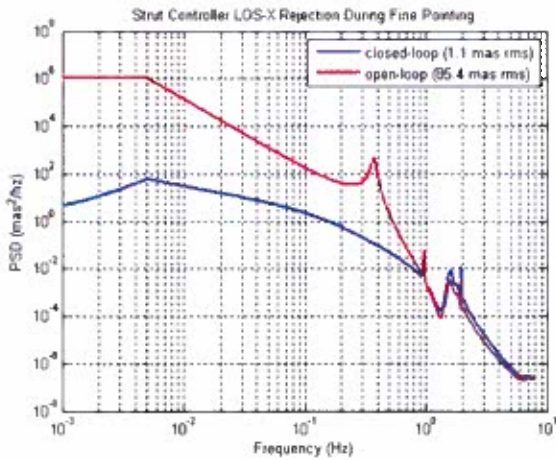


Figure 20. APSI Hexapod Pointing Closed Loop and Open Loop Transfer Functions.

The active isolator compensator offloads the FSM loop to maximize the range of travel for FSM. Controller synthesis is based on a high-fidelity continuous-time open loop FEM with 1330 modes. Continuous time controller employs a series of lead-lag compensators and a bending filter. The controller is a 2×2 transfer function with identical entries along the diagonal and zero entries elsewhere. With sampling time finalized the controller will be in discrete time domain with similar frequency characteristics including stability margins. The design is optimized for spacecraft induced disturbance rejection. Robustness metrics meet NGAS design-to goals of 10 dB gain margin and 30 deg phase margins. Margins were computed using unreduced plant with 2660 states. Similar margins are achieved for both control channels. Closed vs. open loop LOS transfer functions are shown below to exhibit significant attenuation below 1 Hz with active isolation.

SC rX to LOS X



SC rY to LOS Y

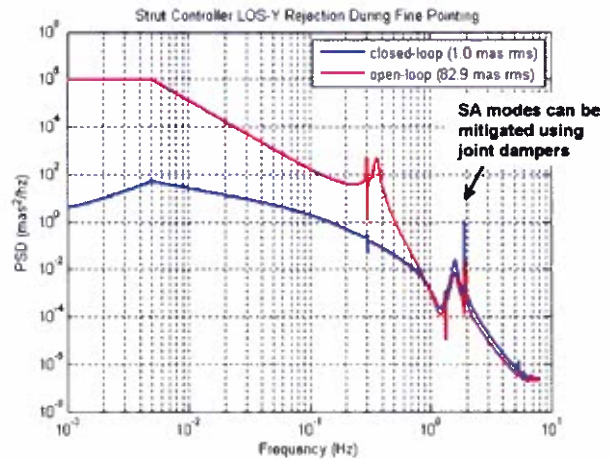


Figure 21. APSI Disturbance Rejection Capability

A detailed FEM of the CSI active/passive isolator has been included in the ACCESS integrated model to determine on-orbit performance. The model is test validated based on the CSI hardware measurements. An open loop model was generated for this purpose. Actuator commands decouple BW LOS and minimize coupling between LOS responses in the commanded and orthogonal directions. The generalized stiffness of the rocking modes was used to generate a 6×2 transformation matrix for strut control. The method generates unity gain at DC and 4 orders of magnitude of separation

between LOS X and Y. A reduced open Loop Plant was then generated to expedite controller design and analysis run times. This was done using a Balanced Realization technique, truncating the least controllable/observable states. A stable controller design was achieved to provide the required SC disturbance rejection. The closed loop plant of the strut controller demonstrated gain controller margins and verified that strut controller rejection of SC disturbances exceeded the 50:1 rejection requirement, as is seen in Figure 21.

Telescope Pointing Trade Study

JPL performed an independent evaluation of both hexapod options. This evaluation consisted in assessing the closed loop performance for each hexapod. In this process, JPL tuned the controller designs for each option to optimize the performance. For this study, the ACS model described in Section 7 was used.

From the vibration isolation capability point of view, the APSI has better performance than AIMS. However, because of the availability of a dual stage Reaction Wheel Isolator that could reduce the jitter substantially, the pointing performance was seen as the key metric. Based on the improved pointing performance of AIMS, the AIMS was chosen to be the primary option and the APSI to be the secondary option. However, it is recommend carrying both options further since the pointing challenges could vary and both designs are very capable and have their own advantages.

9. CORONAGRAPH POINTING SYSTEM

The coronagraph pointing system includes the fine guidance camera, the fine steering mirror (FSM) and the fine pointing algorithms that command all three stages of pointing control (ACS, hexapod, and FSM). The architecture of this design was described in Section 3. This coronagraph pointing system runs at 100 Hz. The fine guidance camera generates measurements of the line-of-sight tip and tilt errors with respect to the star. This measurement is used to control the FSM and the Hexapod. An advanced control law allows to offload the FSM to the hexapod smoothly and effectively [7]. Basically the FSM loop has a high bandwidth compensator that responds quickly to pointing errors, and the hexapod has a mid bandwidth compensator that responds slower and offloads the FSM.

In turn, the hexapod is offloaded to the spacecraft ACS by generating a highly accuracy offset angle derived from the hexapod pointing angles. Assuming the hexapod is tracking the guide star with a precision of 1 mas (1σ) means that the hexapod pointing angles are the opposite of the spacecraft pointing error to the tracking performance level 1 mas (1σ). A measurement of the hexapod pointing angles derived from measurements of the lengths of the hexapod struts is used to generate the offset pointing command for the ACS. The hexapod has a closed loop bandwidth of about 5 Hz which allows it to reject ACS errors with frequencies bellow 0.5 Hz. In addition the FSM has a closed loop bandwidth of 15 Hz, which allows it to correct for some residual errors at the hexapod stage.

10. SIMULATION

The performance is illustrated via closed loop simulation for tracking of a magnitude 7 star. Figure 8.5.5-50 shows the ACS pointing error. Figure 8.5.5-51 shows the hexapod struts angle in the sky commands. Note that they are the opposite of the pointing errors as expected in the tracking case. Figure 8.5.5-52 shows the telescope LOS pointing error, which is the residual error after the ACS and Hexapod control stages. Figure 8.5.5-53 shows the FSM angle in the sky commands. Here also they are the opposite of the telescope pointing errors as expected. Figure 8.5.5-54 the coronagraph pointing error. Figure 8.5.5-55 shows the fine guidance camera measurement of the coronagraph pointing error.

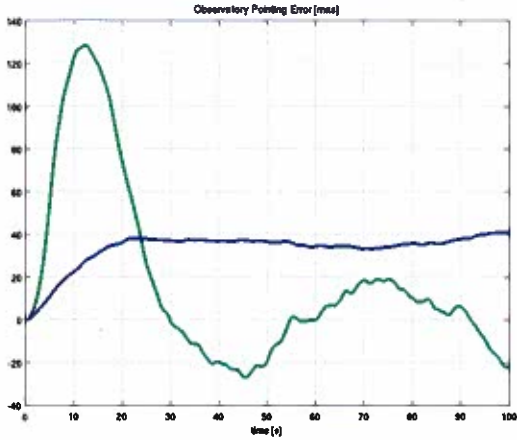


Figure 8. ACS Line-of sight (LOS) Pointing Error

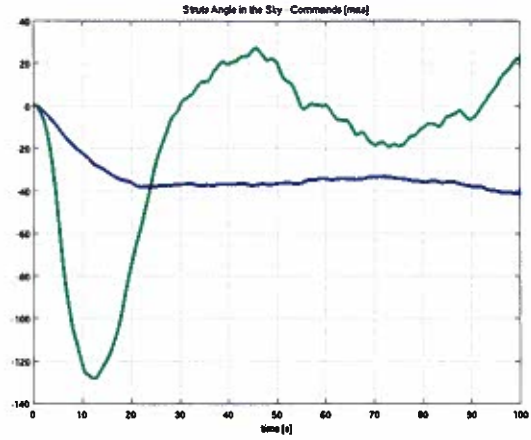


Figure 9. Telescope Pointing System (hexapod) LOS pointing commands.

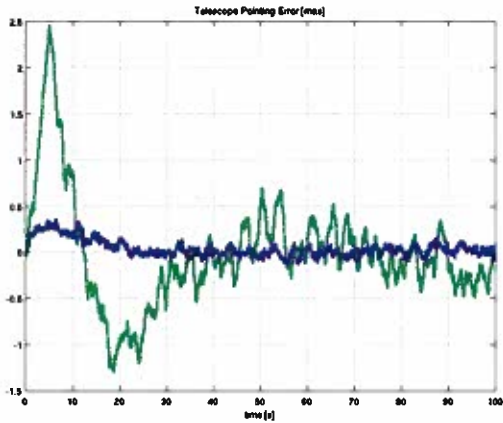


Figure 10. Telescope Pointing System (hexapod) LOS pointing errors.

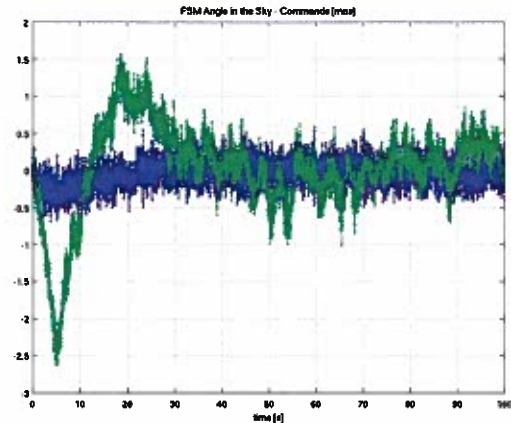


Figure 11. Coronagraph Pointing System (Fine Steering Mirror) LOS pointing commands.

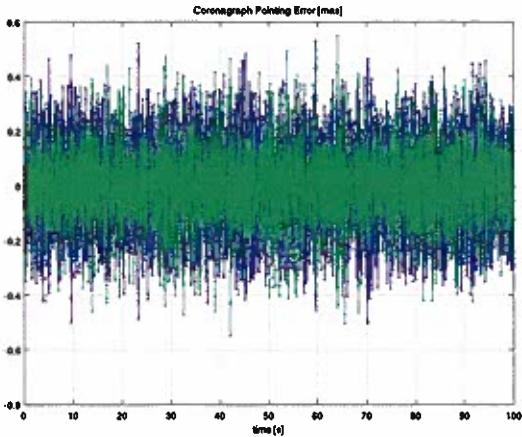


Figure 12. Coronagraph Pointing System (FSM) LOS pointing errors.

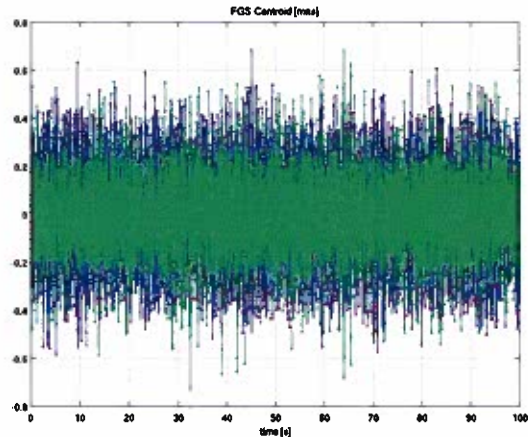


Figure 13. Fine Guidance Camera Centroid Measurements.

11. OPERATIONAL ASPECTS

Pointing Acquisition

The ACCESS PCS employs three steps to achieve the high level of fine pointing performance required to center and maintain the target star on the occulting mask, which is similar to the approach proposed in [1]. This process is depicted in Figure 8.5.6-1. The observatory stability requirement (1.5 arcseconds over 100 seconds), ensures a stable enough environment for successful handoffs between these 3 steps.

The **first step** in fine pointing acquisition uses the SC ACS to point the telescope line-of-sight within 30 arcsec (3 σ) of the target star. The **second step** performs a step-and-stare mosaic search moving the observatory using the SC ACS (Eclipse 2006). The search region for the target star corresponds to uncertainty in the previous step, which corresponds to a 60 \times 60 arcsec region. Since the FGC FOV is 35.8 \times 35.8 arcsec, searching a 60 \times 60 arcsec region requires a 2 \times 2 mosaic allowing for a 5.8 arcsec of overlap. During the search, the hexapod and FSM are held at their reference known position with respect to the observatory. Once the star is found the SC ACS, hexapod and FSM control loops are controlled to their reference positions. In the **third step**, the FGC is transition to the 10 \times 10 pixels tracking window mode and the software engages the high frequency hexapod and FSM control loops, and the generation of the offset pointing signal for the SC Attitude Estimator. This process is expected to take less than 5 minutes. A similar concept has been proposed for SIM-Planetquest [8].

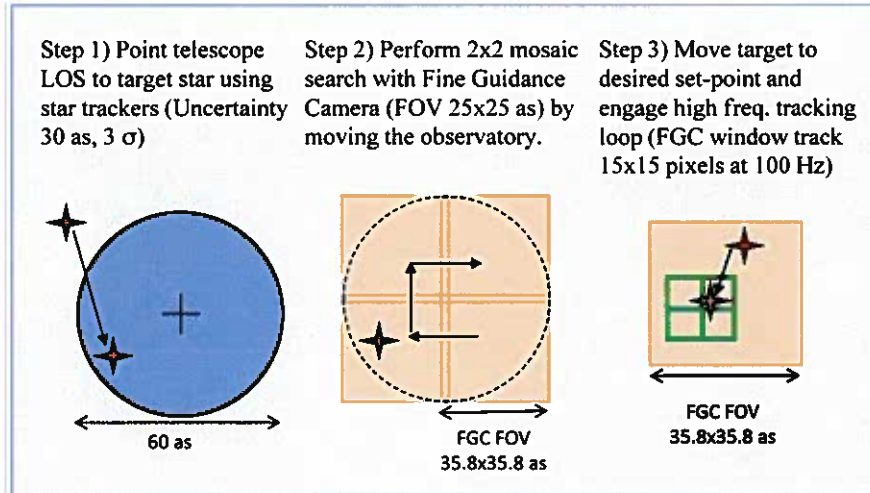


Figure 14. ACCESS pointing acquisition and stabilization strategy ensures placement of the star image on the occulting mask.

Pointing Calibration

Calibration of alignments between the different pointing stages and the science instrument is necessary to achieve the desired performance. An Instrument Pointing Frame filter will be used to estimate the alignments at the beginning of the mission and mid-mission if necessary. Initially it will run during the In-orbit checkout phase [9]. Additionally a star centering calibration algorithm will be run to estimate the misalignment between the FGC predicted occulter center with respect to the actual center as seen in the science images. This filter will be run at the frequency needed to maintain the desired alignment within spec.

12. DISCUSSION AND CONCLUSION

The objective behind this Pointing Control System design has been to propose the best pointing system for a mid-class space coronagraphic observatory with nearly available technology (TRL 6 or above). This study began by setting up a set of pointing goals for the two key science driven pointing requirements: the telescope line-of-sight stability and the star centering on the occulting mask. These goals were set to enable science observations with high contrast at $2\lambda/D$

inner-working-angles. The pointing goals were set to 1 mas (3 sigma) for the telescope line-of-sight stability over 1000s and 0.1 mas (3 sigma) for the star centering on the occulting mask stability over 1000s.

These requirements in conjunction with the design principle to have healthy engineering margins led to include a three stage pointing actuation system; a fine guidance camera design within the coronagraphic instrument; and an extensive disturbance rejection strategy to minimize the environmental jitter.

The three-stage pointing actuation system starts with a standard 3-axis stabilized spacecraft bus and it is augmented with a hexapod telescope pointing system and a fine steering mirror. The addition of the hexapod enables pointing the telescope with a pointing stability ten times better than Hubble but with a spacecraft bus that is ten times less capable than Hubble. Hubble to date has achieved the finest pointing of all NASA space observatories. It has demonstrated a 10 mas (3 sigma) pointing capability. The pointing requirement set for the ACCESS ACS subsystem is 100 mas (3 sigma), which is consistent with mid-class space observatories (Kepler, Spitzer). The second stage is a Telescope Pointing System, the hexapod, allows to reach the 1 mas stability requirement. The third stage is the fine steering mirror, which allows for additional pointing capability within the coronagraphic instrument to center the star on the occulting mask to the 0.1 mas level. If the telescope pointing stability requirement were to be reduced to 10 mas (3 sigma) it could enable to simplify the design by eliminating the Telescope Pointing Control system but will require to optimize the ACS design to achieve Hubble class pointing performance.

For fine guidance sensing we take advantage that coronagraphic observations typically have a bright star in the center of their field of view. We have studied three different concepts for a fine guidance camera that guides from this bright star. This trade study indicated that a Fine Guidance Camera can achieve a pointing knowledge of 0.45 mas (3 sigma) at a sampling rate of 100 Hz for a star magnitude 7 or brighter. Therefore, the pointing requirement for the star centering was relaxed to this value.

The strategy towards disturbances has been to minimize the jitter at the source. We have selected a quiet orbital environment (L2), designed a thermally controlled telescope and instrument, planned operational constraints during science observations (limitations on reaction wheel speeds, non operation of solar array drives and high gain antenna gimbals), and added reaction wheel isolators, solar array dampers and a vibration suppression capability within the hexapod.

Two options for the Telescope Pointing System have been studied, the ITT AIMS system and NG APSI system.

A detail modeling and analysis effort has been performed to evaluate the feasibility and demonstrate the performance of this design. The modeling effort included dynamic models of the structure, optics and models for the spacecraft ACS system, the hexapod pointing systems, the FSM and the fine guidance camera/centroiding. The analysis effort included evaluation of the ACS pointing performance, a trade study between the two telescope pointing system that evaluated the jitter and pointing performance capabilities, and a coronagraph pointing system study that analyzed the multi-stage architecture. The telescope pointing system trade study led to the selection of the ITT AIMS system as the primary option for its improved pointing performance. However, NG APSI had better vibration isolation capabilities. The pointing performance was viewed as the key metric since the vibration isolation requirement on the hexapod could be greatly relaxed by the addition of a dual stage reaction wheel isolator.

The results of this study indicate that additional performance could be gained by:

- Using dual stage reaction wheel isolators.
- Rigidly attaching solar array panels to the telescope body (like in the Spitzer Space Telescope and Kepler) to mitigate Solar Array flexibility interaction with control loops.
- Optimizing the structure to minimize control structure interactions and maximize controllability and vibration suppression.
- Adding magnetic dampers and/or proof mass actuators for local damping.

An important aspect of this mission is its “graceful degradation” to pointing errors. Because the pointing requirements are directly driven from the science instrument occulting mask inner-working-angle, and by this instrument carrying a filter wheel of candidate occulting masks with different inner-working-angles, this mission maintains a reduced science return capability under certain pointing system failures or degraded performance. For example, an 8th order Lyot mask

with a $4\lambda/D$ inner-working-angle [1] relaxes the pointing requirements by nearly two orders of magnitude providing robustness against failures or degraded performance on the telescope or coronagraph pointing elements.

In conclusion, we propose a robust high precision Pointing Control System for the ACCESS Mission concept. A design based on nearly available technologies (TRL >6) with limited complexity.

Acknowledgment

This research was carried out at the Jet Propulsion Laboratory, California Institute of Technology, under a contract with the National Aeronautics and Space Administration.

REFERENCES

- [1] Brugarolas, P. B., Kia, T., Li, D., and Alexander, J. W. "Pointing control system for the Eclipse mission," Proc. SPIE 6265, 62653 (2006).
- [2] Mayo, R. A., Spector, V. A., and Lillie, C. F. "Pointing and jitter control for the Eclipse mission," Proc. SPIE 4854, 544–553. (2003).
- [3] Guyon, O., Matsuo, T., and Angel, R. "Coronagraphic Low Order Wavefront Sensor: Principle and Application to a Phase-Induced Amplitude Coronagraph," *The Astrophysical Journal* 693(1): 75–84. (2009).
- [4] Hopkins, M. A., Smith, D. A., Vallone, P., et al. "Hybrid multivariable controller architecture," Proc. SPIE 5760, 390–401. (2005).
- [5] Vallone, P., and Hopkins, M. A. "Experimental verification of a novel system ID technique called pseudolinear identification (PLID) using a flexible 3D structure," Proc. SPIE 2442, 241–254. (1995).
- [6] Vallone, P. "High-performance piezo-based self-sensor for structural vibration control," Proc. SPIE 2443, 643–655. (1995).
- [7] Lurie, B. J., and Enright, P. J. [Classical Feedback Control with MATLAB]. Marcel Dekker, NY. (2000).
- [8] Brugarolas, P. B., and Kang, B. H. "Instrument pointing control system for the Stellar Interferometry Mission: Planet Quest," Proc. SPIE 6268, 626825 (2006).
- [9] Bayard, D. S., Kang, B. H., Brugarolas, P. B., and Boussalis, D. "An integrated optimal estimation approach to Spitzer Space Telescope focal plane survey," Proc. SPIE 5487, 146–157. (2004).
- [10] Phillip Vallone, Robert M. Egerman, and Jason Elias, "Active dynamic isolation and pointing control system design and analysis for the ACCESS TPF mission concept," to appear in Proc. SPIE Symposium on SPIE Astronomical Telescopes and Instrumentation, June-July 2010, Paper 7738-67, San Diego, California.
- [11] John Nella et al., "James Webb Space Telescope (JWST) Observatory Architecture and Performance" in Proc. Space 2004, AIAA 2004-5086 (2004).
- [12] Allen J. Bronowicki, "A layered vibration control strategy for space telescopes," in Proc. SPIE, Vol. 5056, 487 (2003).
- [13] Vanessa Camelo et al. ,"Damping and Isolation Concepts for Vibration Suppression and Pointing Performance," in Proc. 50th AIAA/ASME/ASCE/AHS/ASC Structures, Structural Dynamics, and Materials Conference, AIAA 2009-2637 (2009).
- [14] John Trauger et al., "ACCESS: a NASA mission concept study of an Actively Corrected Coronagraph for Exoplanet System Studies," in Proc. SPIE Vol 7010, 701029-10.
- [15] John Trauger et al., "ACCESS: a concept study for the direct imaging and spectroscopy of exoplanetary systems," to appear in Proc SPIE, Paper 7731-79 of Conference 7731. July 2010.

JPL SECTION 343 TECHNICAL PEER REVIEW EVALUATION FORM**Author/Phone: Paul Brugarolas, 4-9243****Manuscript Title: ACCESS Pointing Control System****Publication: SPIE Astronomical Instrumentation****Reviewer/Phone: David S. Bayard, 4-8208****Guidelines (URL):****Reviewer Comments:**

This paper presents a new pointing control system architecture designed to support the ACCESS mission proposal. ACCESS is a space coronagraph for exoplanet exploration and discovery. To support such a mission, the pointing performance has to be 10 times better than the Hubble Space Telescope. This challenge is addressed by using a new pointing system architecture comprised of a 3-axis stabilized spacecraft augmented with a hexapod-controlled telescope platform and a fine steering mirror. In addition, the equivalent of a fine guidance sensor is constructed from the coronagraphic observation itself using the fortunate fact that, to support science, there is always a bright star (being nulled) exactly in the center of the coronagraph field of view. A simulation study summarizes the performance of the pointing system to be better than 1 milliarcsecond. This paper presents an example of an aggressive telescope mission using state-of-the-art spacecraft pointing concepts, and serves as a fine addition to the literature.

Author's Responses:**Reviewer's Signature and Date:**

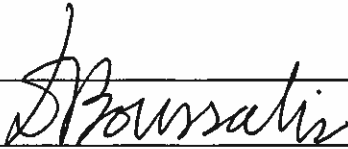
June 2, 2010

Hours Spent in Review (can be logged as Training Time): 1 Hour

July 2006

NOTE: The paper and documented technical peer reviews (at least two) shall be provided to Section Management for their review and approval prior to submittal to Document Review (along with JPL Form 1330)

JPL SECTION 343 TECHNICAL PEER REVIEW EVALUATION FORM

Author/Phone: Paul Brugarolas / 4-9243	
Manuscript Title: ACCESS Pointing Control	
Publication: JPL Report Site	
Reviewer/Phone: Dhemitrios Boussalis / 4-3977	
Guidelines (URL):	
Reviewer Comments: <p>This document presents the architecture, design and performance evaluation result of a high-precision pointing control system for the ACCESS coronagraph mission. This is an innovative three-stage system to achieve stringent pointing accuracy requirements. This particular mission requires that errors of the order of 1-2 arcsec induced by the ACS be compensated so that at the third (fine) stage, a fast-steering mirror can provide the desired accuracy of 0.1 msec. The intermediate stage employs an actively controlled hexapod on which the instrument is mounted.</p> <p>The author gives an excellent presentation of his approach, which resulted in the successful design of a high-precision pointing control system. The pointing performance is demonstrated via a high-fidelity computer simulation.</p> <p>This paper will undoubtedly generate a lot of interest among astronomers and controls engineers.</p>	
Author's Responses:	
Reviewer's Signature and Date:	 6/3/2010
Hours Spent in Review (can be logged as Training Time): 1 Hour	

July 2006

NOTE: The paper and documented technical peer reviews (at least two) shall be provided to Section Management for their review and approval prior to submittal to Document Review (along with JPL Form 1330)